J. Fluid Mech. (2013), *vol.* 718, *pp.* 347–370. © Cambridge University Press 2013
doi:10.1017/jfm.2012.616

Lattice ellipsoidal statistical BGK model for thermal non-equilibrium flows

Jianping Meng[1], Yonghao Zhang[1,†], Nicolas G. Hadjiconstantinou[2], Gregg A. Radtke[2] and Xiaowen Shan[3]

[1]Department of Mechanical & Aerospace Engineering, University of Strathclyde, Glasgow G1 1XJ, UK

[2]Department of Mechanical Engineering, Massachusetts Institute of Technology, Cambridge, MA 02139, USA

[3]Beijing Aeronautical Science & Technology Research Institute, Commercial Aircraft Corporation of China, Ltd, Beijing, 102211, China

(Received 10 April 2012; revised 28 September 2012; accepted 11 December 2012; first published online 8 February 2013)

A thermal lattice Boltzmann model is constructed on the basis of the ellipsoidal statistical Bhatnagar–Gross–Krook (ES-BGK) collision operator via the Hermite moment representation. The resulting lattice ES-BGK model uses a single distribution function and features an adjustable Prandtl number. Numerical simulations show that using a moderate discrete velocity set, this model can accurately recover steady and transient solutions of the ES-BGK equation in the slip-flow and early transition regimes in the small-Mach-number limit that is typical of microscale problems of practical interest. In the transition regime in particular, comparisons with numerical solutions of the ES-BGK model, direct and low-variance deviational Monte Carlo simulations show good accuracy for values of the Knudsen number up to approximately 0.5. On the other hand, highly non-equilibrium phenomena characterized by high Mach numbers, such as viscous heating and force-driven Poiseuille flow for large values of the driving force, are more difficult to capture quantitatively in the transition regime using discretizations chosen with computational efficiency in mind such as the one used here, although improved accuracy is observed as the number of discrete velocities is increased.

Key words: computational methods, kinetic theory, micro-/nano-fluid dynamics

1. Introduction

The lattice Boltzmann (LB) method has been successful in simulating isothermal (athermal) flows; however, thermal flows still remain a challenge, despite significant efforts from a number of research groups (see Chen & Doolen 1998; Lallemand & Luo 2003; Watari & Tsutahara 2003; Gonnella, Lamura & Sofonea 2007; Guo *et al.* 2007; Prasianakis & Karlin 2007; Shan & Chen 2007; Prasianakis & Karlin 2008; Prasianakis *et al.* 2009; Sbragaglia *et al.* 2009; Watari 2009; Scagliarini *et al.* 2010; Zheng *et al.* 2010; Shim & Gatignol 2011). Recent approaches fall into two broad categories: the high-order approach (e.g. Watari & Tsutahara 2003; Shan &

† Email address for correspondence: yonghao.zhang@strath.ac.uk

https://doi.org/10.1017/jfm.2012.616 Published online by Cambridge University Press

Chen 2007; Sbragaglia *et al.* 2009) and the double-distribution-function approach (e.g. Shan 1997; He, Chen & Doolen 1998). As a direct extension of the isothermal LB model, the high-order model only uses one distribution function while retaining high-order terms in the equilibrium distribution function to recover the full Navier–Stokes (NS) equations. Unfortunately, this approach requires a richer velocity space and as a result suffers in terms of simplicity and in some cases numerical instability. By contrast, in the double-distribution-function approach, two distribution functions are utilized: one for the velocity field and the other for the temperature field. As a result, high-order terms can be avoided and the standard lattice can be used. In addition, this approach is numerically more stable. However, to utilize the standard lattice, the energy and momentum transport equation need to be decoupled through the Boussinesq approximation (cf. Guo *et al.* 2007); in this case, the double-distribution approach does not recover the full NS equations in a strict sense. In addition to these two approaches, we also note some efforts on constructing single-distribution-function thermal models using standard lattices, e.g. a two-dimensional model with nine discrete velocities (see Prasianakis & Karlin 2007).

In addition to heat transfer, kinetic effects can make flows even more complex. For example, for gaseous flows at the microscale, kinetic effects have to be taken into account as the Knudsen number (*Kn*, the ratio of the mean free path to the characteristic length) becomes finite (Hadjiconstantinou 2006). Due to its kinetic origins, the LB method has been shown to be able to describe moderately complex kinetic effects (see e.g. Succi 2002; Sbragaglia & Succi 2005; Toschi & Succi 2005; Zhang, Qin & Emerson 2005; Sbragaglia & Succi 2006; Shan, Yuan & Chen 2006; Guo, Zhao & Shi 2006; Zhang *et al.* 2006; Ansumali *et al.* 2007; Tian *et al.* 2007; Kim, Pitsch & Boyd 2008*a*,*b*; Tang *et al.* 2008*a*; Tang, Zhang & Emerson 2008*b*; Yudistiawan, Ansumali & Karlin 2008). Particularly, as the LB method can be considered as an approximation to the Boltzmann–BGK equation, high-order models should, in principle, be able to go beyond NS hydrodynamics (Shan *et al.* 2006; Meng & Zhang 2011*a*). Both analytical and numerical analysis have shown that using an appropriate discrete velocity set, LB models can capture kinetic effects including the Knudsen layer qualitatively and provide reasonably accurate results for a range of isothermal problems (Kim *et al.* 2008*a*; Yudistiawan *et al.* 2008); also, as expected, more discrete velocities generally give better predictions (Meng & Zhang 2011*a*). When gas–surface interactions are concerned, discrete velocity sets from even-order Hermite polynomials typically perform better (Meng & Zhang 2011*b*). For thermal rarefied flows, despite the velocity-slip and temperature-jump problems having been investigated using a high-order LB model (Watari 2009), significant effort is still required to develop robust LB methods for modelling general non-equilibrium flows of engineering interest.

The Hermite expansion provides a systematic approach for deriving LB models of the NS system of equation and beyond (Shan *et al.* 2006). The usage of the Hermite expansion was pioneered by Grad (1949, 1958) for approximating solutions to the Boltzmann equation. An important feature of Hermite polynomials is that the expansion coefficients correspond directly to moments of the distribution function. In addition, the truncation of higher-order terms does not directly alter the lower-order velocity moments of the distribution function. In his famous paper, Grad kept the first thirteen Hermite coefficients and obtained the well-known 13-moment system (Grad 1949). This system contains physics beyond the NS equation. However, a significant weakness of Grad's 13-moment system is its inability to describe smooth shock structures above a critical Mach number. Also, this system is not easily related *a*

https://doi.org/10.1017/jfm.2012.616 Published online by Cambridge University Press

priori to the Knudsen number. As a result, significant effort has been devoted towards the development of an improved moment system in the last decade. Regularization for Grad's 13-moment system (i.e. the so-called R13 system) has been introduced on the basis of a Chapman–Enskog expansion around a non-equilibrium state (Struchtrup & Torrilhon 2003; Struchtrup 2004, 2005*a*). The related issues associated with the numerical scheme and boundary conditions have then been discussed by Gu & Emerson (2007) and Torrilhon & Struchtrup (2008). A series of analytical solutions were also obtained and compared to the kinetic solutions (see Taheri, Torrilhon & Struchtrup 2009; Taheri & Struchtrup 2010). In addition to the R13 system, higher-order moment-equation models have also been developed (Gu & Emerson 2009).

Inspired by Grad's work, the Hermite expansion has been used to derive new LB models (Shan & He 1998; Shan *et al.* 2006). It was shown that the truncation of the Hermite expansion is equivalent to evaluating the distribution function at the chosen order of the discrete velocities. Thus, the resulting LB models can describe gaseous systems at the corresponding level. However, compared to Grad's approach, the governing equation of LB models is in a much simpler form (e.g. the linear convective term) as the evolution is accomplished at the distribution-function level rather than the state-variable level. Therefore, the LB model has some advantages, e.g. straightforward numerical implementation and code parallelization.

In this work, we establish a thermal LB model based on the ellipsoidal statistical Bhatnagar–Gross–Krook (ES-BGK) equation following the systematic procedure of high-order Hermite expansion. The resulting model features an adjustable Prandtl number in contrast to the BGK model whose Prandtl number is fixed at 1. We validate our model using shear-driven (Couette) flows, Fourier flows and unsteady boundary heating problems in the small-Mach-number limit over a range of Knudsen numbers. Using only a moderate set of discrete velocities, we find very good agreement with benchmark solutions. We also show that, with the same moderate discrete velocity set, highly non-equilibrium problems characterized by high Mach numbers, such as force-driven Poiseuille flow for large values of the driving force, are captured accurately in the slip-flow regime and with good qualitative accuracy in the transition regime. Better accuracy requires a higher number of discrete velocities, in addition to higher-order Hermite expansion.

2. Thermal lattice Boltzmann model

2.1. *The ES-BGK equation*

The difficulty associated with solving the Boltzmann equation is mainly due to the collision term. To reduce the complexity, the collision term may be replaced by a simple statistical model that preserves the conservation laws of mass, momentum and energy. The most commonly used model is known as the Bhatnagar–Gross–Krook (BGK) collision operator, which is often used in constructing lattice Boltzmann models. Despite its success, the BGK model suffers from a number of drawbacks: specifically, it yields a fixed Prandtl number (Pr) of unity, while the correct value for a monatomic gas is close to 2/3. To address this limitation, Holway (1966) proposed the ES-BGK model which replaces the Maxwellian distribution of the standard BGK equation with an anisotropic Gaussian distribution. This model can be written as

$$\frac{\partial \hat{f}}{\partial \hat{t}} + \hat{c}_i \frac{\partial \hat{f}}{\partial \hat{x}_i} + \hat{g}_i \frac{\partial \hat{f}}{\partial \hat{c}_i} = -\frac{1}{\hat{\tau}}(\hat{f} - \hat{f}_{ES}), \tag{2.1}$$

https://doi.org/10.1017/jfm.2012.616 Published online by Cambridge University Press

where $\hat{f}$ denotes the single-particle distribution function, $\hat{c}_i$ the phase (particle) velocity, $\hat{g}_i$ the body force and $\hat{\tau}$ the mean relaxation time which is assumed to be independent of particle velocity. The anisotropic Gaussian distribution can be written as

$$\hat{f}_{ES} = \hat{\rho}\frac{1}{\sqrt{\det[2\pi\hat{\lambda}_{ij}]}}\exp\left[-\frac{1}{2}\hat{\lambda}_{ij}^{-1}\hat{C}_i\hat{C}_j\right], \tag{2.2}$$

where $\hat{\lambda}_{ij} = R\hat{T}\delta_{ij} + (b\hat{\sigma}_{ij})/\hat{\rho}$ and R is the gas constant. Macroscopic quantities, such as density $\hat{\rho}$, velocity $\hat{\boldsymbol{u}}$, shear stress $\hat{\boldsymbol{\sigma}}$, temperature $\hat{T}$ and heat flux $\hat{\boldsymbol{q}}$, can be obtained by integrating the distribution function over the velocity space, i.e.

$$\begin{bmatrix} \hat{\rho} \\ \hat{\rho}\hat{u}_i \\ \hat{\sigma}_{ij} \\ \hat{q}_i \\ \hat{\rho}DR\hat{T} \end{bmatrix} = \int \hat{f} \begin{bmatrix} 1 \\ \hat{c}_i \\ \hat{C}_{<i}\hat{C}_{j>} \\ \frac{1}{2}\hat{C}_i\hat{C}_j\hat{C}_j \\ \hat{C}_i\hat{C}_i \end{bmatrix} \mathrm{d}\hat{\boldsymbol{c}}, \tag{2.3}$$

where $\hat{C}_i = \hat{c}_i - \hat{u}_i$ is the particle peculiar velocity, D is the spatial dimension and the angle brackets denote trace-free tensors (see Struchtrup 2005*b*, Appendix A.2.2). The pressure $\hat{p}$ can be related to the density and temperature by the equation of state

$$\hat{p} = \hat{\rho}R\hat{T}. \tag{2.4}$$

As $\hat{\lambda}_{ij}^{-1}$ (the inverse of the matrix) must be positive definite, b is restricted to $-1/2 \leqslant b \leqslant 1$. The exact values of b and $\hat{\tau}$ can be determined from theory for known inter-molecular force laws or experimental data. In this work, experimental values will be used. The Navier–Stokes equations can be derived (Holway 1966) using a Chapman–Enskog expansion. The viscosity and thermal conduction coefficients can be written as $\hat{\mu} = (\hat{p}\hat{\tau})/(1-b)$ and $\hat{\kappa} = \hat{p}R(D+2)\hat{\tau}/2$, respectively. Therefore, the Prandtl number is given by $Pr = 1/(1-b)$ and can be adjusted via the free parameter b. For thermal flows, viscosity depends on temperature, and can be expressed as $\hat{\mu}/\mu_0 = (\hat{T}/T_0)^{\varpi}$, where ϖ is related to the molecular interaction model, varying from 0.5 for hard-sphere molecular interactions to 1 for Maxwellian interactions. Therefore, in general, $\hat{\tau}$ may be taken to be a function of temperature.

The ES-BGK model has received renewed attention, in part because the associated H theorem was recently proven (Andries *et al.* 2000). Several studies have shown that it can provide reasonable accuracy for modelling transport in simple rarefied flows (Garzó & Santos 1995; Andries *et al.* 2002; Mieussens & Struchtrup 2004; Han *et al.* 2007; Graur & Polikarpov 2009; Gallis & Torczynski 2011; Han, Muntz & Alexeenko 2011). In the following, we will develop a thermal LB model based on the ES-BGK equation using the Hermite moment representation (Shan *et al.* 2006); we will refer to the resulting LB method as the lattice ES-BGK model. In order to separate the numerical error arising from the LB method from the modelling error associated with approximating the hard-sphere operator with the ES-BGK model, we will also present *numerical* solutions of the Boltzmann equation with the ES-BGK collision operator obtained using the finite-difference/discrete-velocity method presented in Aoki, Takata & Nakanishi (2002). Although this method is not practical for problems of engineering interest due to the high dimensionality associated with the very fine discretization of the velocity space, it can be used to obtain accurate solutions of the ES-BGK

https://doi.org/10.1017/jfm.2012.616 Published online by Cambridge University Press

equation in the one-dimensional benchmark problems considered here. In order to differentiate from our lattice-based solutions, we will refer to the ones obtained by the finite-difference/discrete-velocity method as *numerical*.

2.2. *Derivation of the lattice ES-BGK equation*

Shan *et al.* (2006) have shown that a hierarchy of different-order LB models can be systematically derived from the BGK equation via the Hermite expansion, which can be regarded as approximations to the BGK equation. Gas flows can then be described at the kinetic level with various discrete velocity sets. This procedure can also be used to derive the lattice ES-BGK model. For convenience, we use the following non-dimensional system:

$$\left.\begin{aligned} x_i = \frac{\hat{x}_i}{L}, \quad u_i = \frac{\hat{u}_i}{\sqrt{RT_0}}, \quad t = \frac{\sqrt{RT_0}\hat{t}}{L}, \\ g_i = \frac{L\hat{g}_i}{RT_0}, \quad c_i = \frac{\hat{c}_i}{\sqrt{RT_0}}, \quad T = \frac{\hat{T}}{T_0}, \end{aligned}\right\} \tag{2.5}$$

$$\left.\begin{aligned} \tau = \frac{\sqrt{RT_0}\hat{\tau}}{L}, \quad f = \frac{\hat{f}\,(RT_0)^{D/2}}{\rho_0}, \quad \rho = \frac{\hat{\rho}}{\rho_0}, \quad p = \frac{\hat{p}}{p_0}, \\ \mu = \frac{\hat{\mu}}{\mu_0}, \quad q_i = \frac{\hat{q}_i}{p_0\sqrt{RT_0}}, \quad \sigma_{ij} = \frac{\hat{\sigma}_{ij}}{p_0}. \end{aligned}\right\} \tag{2.6}$$

where L is the characteristic length of the system and the subscript 0 denotes the reference values of corresponding state variables. The temperature and state equations become

$$DT = \frac{1}{\rho}\int f\, C_i C_i \,\mathrm{d}\boldsymbol{c}, \tag{2.7}$$

$$p = \rho T. \tag{2.8}$$

The non-dimensional relaxation time can be written explicitly as

$$\tau = \frac{\mu_0\sqrt{RT_0}}{p_0 L}\frac{\mu}{Prp} = \frac{Kn}{Pr}\frac{\mu}{p}, \tag{2.9}$$

where the Knudsen number is defined by

$$Kn = \frac{\mu_0\sqrt{RT_0}}{p_0 L}. \tag{2.10}$$

To solve (2.1), the distribution function is first projected onto a functional space spanned by the Hermite basis. If a Gauss–Hermite quadrature of a degree $\geqslant 2N$ is chosen, then the first N velocity moments of the distribution function are retained (see Shan *et al.* 2006, p. 420). Therefore, the distribution function is essentially approximated as

$$f(\boldsymbol{x}, \boldsymbol{c}, t) \approx \omega(\boldsymbol{c}) \sum_{n=0}^{N} \frac{1}{n!}\boldsymbol{a}^{(n)}(\boldsymbol{x}, t) : \boldsymbol{\chi}^{(n)}(\boldsymbol{c}), \tag{2.11}$$

and the coefficients $\boldsymbol{a}^{(n)}$ are calculated from

$$\boldsymbol{a}^{(n)} = \int f \boldsymbol{\chi}^{(n)} \,\mathrm{d}\boldsymbol{c} \tag{2.12}$$

where $\boldsymbol{\chi}^{(n)}$ is the nth-order Hermite polynomial and $\omega(\boldsymbol{c})$ is the weight function.

https://doi.org/10.1017/jfm.2012.616 Published online by Cambridge University Press

The key step is to expand the anisotropic Gaussian distribution as

$$f_{ES} \approx f_{ES}^{N} = \omega(\boldsymbol{c}) \sum_{n=0}^{N} \frac{1}{n!} \boldsymbol{a}_{ES}^{(n)} : \boldsymbol{\chi}^{(n)}(\boldsymbol{c}), \tag{2.13}$$

where

$$\boldsymbol{a}_{ES}^{(n)} = \int f_{ES} \boldsymbol{\chi}^{(n)} \, \mathrm{d}\boldsymbol{c} \approx \sum_{\alpha=1}^{d} \frac{w_\alpha}{\omega(\boldsymbol{c}_\alpha)} f_{ES}^{N} \boldsymbol{\chi}^{n}(\boldsymbol{c}_\alpha), \tag{2.14}$$

and w_α and $\boldsymbol{c}_\alpha$, $\alpha = 1, \ldots, d$, are the weights and abscissae of a Gauss–Hermite quadrature. For the anisotropic distribution, the first a few coefficients are given by

$$a_{ES}^{(0)} = \rho, \tag{2.15}$$

$$a_{ES,i}^{(1)} = \rho u_i, \tag{2.16}$$

$$a_{ES,ij}^{(2)} = \rho(u_i u_j + \lambda_{ij} - \delta_{ij}), \tag{2.17}$$

$$a_{ES,ijk}^{(3)} = \rho(u_i u_j u_k + \lambda_{ij} u_k + \lambda_{ik} u_j + \lambda_{jk} u_i - \delta_{ij} u_k - \delta_{ik} u_j - \delta_{jk} u_i), \tag{2.18}$$

$$\begin{aligned} a_{ES,ijkl}^{(4)} = \rho[&u_i u_j u_l u_k + (\lambda_{il} - \delta_{il}) u_j u_k + (\lambda_{ij} - \delta_{ij}) u_l u_k + (\lambda_{ik} - \delta_{ik}) u_j u_l \\ &+ (\lambda_{jl} - \delta_{jl}) u_i u_k + (\lambda_{jk} - \delta_{jk}) u_i u_l + (\lambda_{kl} - \delta_{kl}) u_i u_j \\ &+ (\lambda_{ij} - \delta_{ij})(\lambda_{kl} - \delta_{kl}) + (\lambda_{ik} - \delta_{ik})(\lambda_{jl} - \delta_{jl}) + (\lambda_{il} - \delta_{il})(\lambda_{kj} - \delta_{kj})]. \end{aligned} \tag{2.19}$$

The body force term $F(\boldsymbol{x}, \boldsymbol{c}, t) = -\boldsymbol{g} \cdot \nabla_c f$ can be approximated as

$$F(\boldsymbol{x}, \boldsymbol{c}, t) = \omega \sum_{n=1}^{N} \frac{1}{(n-1)!} \boldsymbol{g} \boldsymbol{a}^{(n-1)} : \boldsymbol{\chi}^{(n)}. \tag{2.20}$$

Although (2.2) has an infinite Hermite expansion, an LB model is built under the assumption that to some level of approximation only the leading terms contribute explicitly to the hydrodynamics (see Shan *et al.* 2006) and thus the infinite series can be truncated. In this work, a fourth-order Hermite expansion will be used.

Given the above discussion, the ES-BGK equation (2.1) can be rewritten in its truncated form, i.e.

$$\frac{\partial f}{\partial t} + c_i \frac{\partial f}{\partial x_i} = -\frac{1}{\tau}(f - f_{ES}^{N}) + F. \tag{2.21}$$

For a fourth-order expansion, a discrete velocity set with ninth-order or higher accuracy is required (Shan *et al.* 2006). There are a number of ways of constructing a high-order discrete velocity set (Shan *et al.* 2006; Chikatamarla & Karlin 2006, 2009; Shan 2010). A straightforward approach is to utilize the roots of the Hermite polynomial. In one dimension, the discrete velocities c_α are just the roots of the Hermite polynomials, and the corresponding weights are determined by

$$w_\alpha = \frac{n!}{[n\chi^{n-1}(c_\alpha)]^2}. \tag{2.22}$$

Another useful procedure is to utilize the entropy construction (cf. Chikatamarla & Karlin 2006, 2009). Given one-dimensional velocity sets, those of the higher-dimension can be constructed using 'production' formulae (Shan *et al.* 2006). Once the discrete velocity set is chosen, the governing equation of the lattice ES-BGK

https://doi.org/10.1017/jfm.2012.616 Published online by Cambridge University Press

model can be written as

$$\frac{\partial f_\alpha}{\partial t} + c_{\alpha,i}\frac{\partial f_\alpha}{\partial x_i} = -\frac{1}{\tau}\left(f_\alpha - f_{ES,\alpha}\right) + g_\alpha, \tag{2.23}$$

where

$$f_\alpha = \frac{w_\alpha f(\boldsymbol{x}, \boldsymbol{c}_\alpha, t)}{\omega(\boldsymbol{c}_\alpha)}, \quad f_{ES,\alpha} = \frac{w_\alpha f_{ES}(\boldsymbol{x}, \boldsymbol{c}_\alpha, t)}{\omega(\boldsymbol{c}_\alpha)}, \quad g_\alpha = \frac{w_\alpha F(\boldsymbol{x}, \boldsymbol{c}_\alpha, t)}{\omega(\boldsymbol{c}_\alpha)}. \tag{2.24}$$

2.3. *Remarks on the accuracy beyond Navier–Stokes*

As the distribution functions f and f_{ES} are approximated and evaluated at the Gauss–Hermite quadrature points, cf. (2.11), we can relate the chosen Gauss–Hermite quadrature to the approximated moments of the distribution function. Generally speaking, more discrete velocities mean that higher-order moments can be obtained more accurately. With sufficiently accurate quadrature and retaining increasingly high-order terms of the expanded f_{ES}, the LB model is becoming a better approximation of the original ES-BGK equation (cf. figure 19).

When the Chapman–Enskog expansion is valid, we can evaluate model accuracy in terms of the Knudsen number. According to the Chapman–Enskog expansion, the distribution function f is assumed to be given by an asymptotic series expanded in powers of the (formal) small parameter ϵ (see Struchtrup 2005*b*, ch. 4),

$$f = f^{(0)} + \epsilon f^{(1)} + \epsilon^2 f^{(2)} + \cdots \tag{2.25}$$

where ϵ plays the role of the Knudsen number; $f^{(0)}$ is the Hermite approximation of the Maxwellian f_M (its first four Hermite coefficients can be found in Shan *et al.* 2006, cf. (3.12) therein). Furthermore, the time and spatial variations are also measured in powers of ϵ, i.e.

$$\partial_t = \epsilon\partial_t^{(0)} + \epsilon^2\partial_t^{(1)} + \cdots \tag{2.26}$$

and $\boldsymbol{\nabla} = \epsilon\boldsymbol{\nabla}$ (Shan *et al.* 2006). Considering the form of f^0, f_{ES}^N can be written as

$$f_{ES}^N = f^{(0)} + \omega\left[\tfrac{1}{2}b\sigma_{ij}\chi_{ij}^{(2)} + \tfrac{1}{6}(\sigma_{ij}u_k + \sigma_{ik}u_j + \sigma_{jk}u_i)\chi_{ijk}^{(3)} + \cdots\right]. \tag{2.27}$$

The shear stress σ_{ij} should be also expanded as

$$\sigma_{ij} = \epsilon\sigma_{ij}^{(1)} + \epsilon^2\sigma_{ij}^{(2)} + \cdots, \tag{2.28}$$

and f_{ES}^N can thereby be written as

$$f_{ES}^N = f^{(0)} + \epsilon f_{ES}^{N,(1)} + \epsilon^2 f_{ES}^{N,(2)} + \cdots, \tag{2.29}$$

where

$$f_{ES}^{N,(1)} = \omega\left[\tfrac{1}{2}b\sigma_{ij}^{(1)}\chi_{ij}^{(2)} + \tfrac{1}{6}(\sigma_{ij}^{(1)}u_k + \sigma_{ik}^{(1)}u_j + \sigma_{jk}^{(1)}u_i)\chi_{ijk}^{(3)} + \cdots\right], \tag{2.30}$$

and

$$f_{ES}^{N,(2)} = \omega\left[\tfrac{1}{2}b\sigma_{ij}^{(2)}\chi_{ij}^{(2)} + \tfrac{1}{6}(\sigma_{ij}^{(2)}u_k + \sigma_{ik}^{(2)}u_j + \sigma_{jk}^{(2)}u_i)\chi_{ijk}^{(3)} + \cdots\right]. \tag{2.31}$$

By matching the terms in the same powers of ϵ, we can have the solution for the two leading orders, namely the NS order

$$f^{(1)} = f_{ES}^{N,(1)} - \tau(\partial_t^{(0)} + \boldsymbol{c}\cdot\boldsymbol{\nabla} + \boldsymbol{g}\cdot\boldsymbol{\nabla}_c)f^{(0)} \tag{2.32}$$

https://doi.org/10.1017/jfm.2012.616 Published online by Cambridge University Press

and the Burnett order

$$f^{(2)} = f_{ES}^{N,(2)} - \tau[(\partial_t^{(0)} + \boldsymbol{c}\cdot\nabla + \boldsymbol{g}\cdot\nabla_c)f^{(1)} + \partial_t^1 f^{(0)}]. \tag{2.33}$$

It is rather tedious to calculate the explicit form of $f^{(1)}$ and $f^{(2)}$. However, here we only need to know their highest order as a Hermite polynomial of the particle velocity $\boldsymbol{c}$. To determine the highest order, we notice that the operators ∂_t^0 and ∂_t^1 do not alter the order while the operators $\boldsymbol{c}\cdot\nabla$ and ∇_c increase the order by one. Therefore, the Burnett-order solution $f^{(2)}$ is a polynomial of $\boldsymbol{c}$ of two-orders higher than f_{ES}^N. If desired, this discussion can be extended to solutions of higher order. Here we restrict the discussion to the first two orders.

With the above discussion, we can estimate the accuracy level associated with the chosen expansion order and quadrature. As fourth-order terms of $\boldsymbol{c}$ are retained in the expansion of f_{ES}, the Burnett-order solution of the distribution function can be represented by a sixth-order polynomial. For the heat flux, a third-order velocity moment, to be calculated with the Burnett level of accuracy, the chosen quadrature has to be accurate for an integration over the full space for a ninth-order polynomial. Hence, according to the Gaussian quadrature rule (cf. Appendix in Shan *et al.* 2006), it is necessary to adopt a quadrature with an algebraic degree of precision beyond the ninth-order. However, as the ninth-order quadrature is not optimal for describing gas–wall interactions (Meng & Zhang 2011*b*), an 11th-order quadrature is chosen in this work.

It is worth noting again that the above analysis relies on the validity of the Chapman–Enskog expansion. Consequently, one should be careful when interpreting the above conclusion for large Knudsen numbers. Furthermore, it may be better to understand the requirement on the quadrature for the corresponding accuracy as necessary rather than sufficient. Nevertheless, the above discussion is useful for understanding the capability of the LB model, which can be seen in numerical simulations below.

3. Numerical implementation

3.1. *Scheme*

To solve (2.23), various numerical schemes can be used, depending on the characteristics of the problem of interest. Typically, if a first-order upwind finite difference is chosen, we have a standard stream-collision scheme.

As flows with various Knudsen numbers will be considered in the following simulations, the numerical scheme has to be carefully chosen to cope with discontinuities at the system boundaries caused by rarefaction (Hadjiconstantinou 2006). In particular, in order to intrinsically describe the gas–surface interaction, the kinetic boundary condition should be accurately implemented in the numerical scheme. Meanwhile, there is still no general and accurate implementation of the standard stream-collision scheme for high-order models, especially for rarefied flows. On the other hand, for high-order LB models, the discrete velocity points may not coincide with the lattice points, which makes the standard stream-collision procedure impossible. Therefore, in the interest of simplicity, a finite-difference formulation has been chosen and more specifically, a first-order forward Euler method is coupled to a second-order total-variation diminishing (TVD) scheme (Kim *et al.* 2008*a*; Sofonea 2009; Toro 2009).

The resulting scheme can be summarized as follows. Let $f_{\alpha,i}^{n,j}$ denote the distribution function value f_α at the node (x_i, y_j) at the nth time step (see figure 1). The distribution

https://doi.org/10.1017/jfm.2012.616 Published online by Cambridge University Press

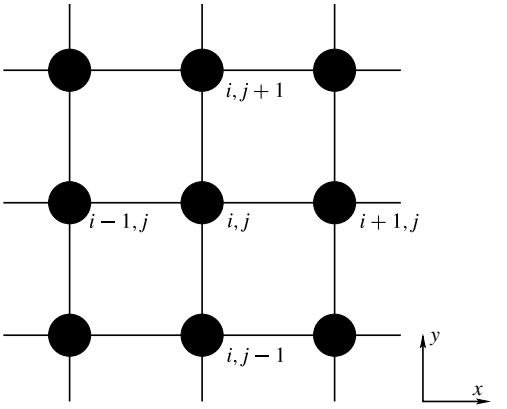


FIGURE 1. Schematic diagram of square lattices.

function update can be written as

$$f_{\alpha,i}^{n+1,j} = f_{\alpha,i}^{n,j} - \frac{c_{\alpha x}\delta_t}{\delta_x}[\mathscr{F}_{\alpha,i+1/2}^{n,j} - \mathscr{F}_{\alpha,i-1/2}^{n,j}] - \frac{c_{\alpha y}\delta_t}{\delta_y}[\mathscr{F}_{\alpha,i}^{n,j+1/2} - \mathscr{F}_{\alpha,i}^{n,j-1/2}]$$
$$+ \frac{\delta_t}{\tau}(f_{\alpha,i}^{ES,n,j} - f_{\alpha,i}^{n,j}) + g_\alpha \delta_t, \tag{3.1}$$

where δ_x and δ_y are the grid spacing in the x and y directions, respectively, and δ_t is the time step; $c_{\alpha x}$ and $c_{\alpha y}$ denote the particle velocity components at the x and y coordinates. The outgoing and incoming fluxes at the node (i, j) (see figure 1) are

$$\mathscr{F}_{\alpha,i+1/2}^{n,j} = f_{\alpha,i}^{n,j} + \frac{1}{2}\left(1 - \frac{c_{\alpha x}\delta_t}{\delta_x}\right)[f_{\alpha,i+1}^{n,j} - f_{\alpha,i}^{n,j}]\Psi\left(\Theta_{\alpha,i}^{n}\right), \tag{3.2}$$

$$\mathscr{F}_{\alpha,i-1/2}^{n,j} = \mathscr{F}_{\alpha,(i-1)+1/2}^{n,j}, \tag{3.3}$$

$$\mathscr{F}_{\alpha,i}^{n,j+1/2} = f_{\alpha,i}^{n,j} + \frac{1}{2}\left(1 - \frac{c_{\alpha y}\delta_t}{\delta_y}\right)[f_{\alpha,i}^{n,j+1} - f_{\alpha,i}^{n,j}]\Psi\left(\Theta_{\alpha}^{n,j}\right), \tag{3.4}$$

$$\mathscr{F}_{\alpha,i}^{n,j-1/2} = \mathscr{F}_{\alpha,i}^{n,(j-1)+1/2}, \tag{3.5}$$

where

$$\Theta_{\alpha,i}^{n} = \frac{f_{\alpha,i}^{n,j} - f_{\alpha,i-1}^{n,j}}{f_{\alpha,i+1}^{n,j} - f_{\alpha,i}^{n,j}}, \tag{3.6}$$

$$\Theta_{\alpha}^{n,j} = \frac{f_{\alpha,i}^{n,j} - f_{\alpha,i}^{n,j-1}}{f_{\alpha,i}^{n,j+1} - f_{\alpha,i}^{n,j}}, \tag{3.7}$$

and the minmod flux limiter is given by

$$\Psi(\Theta) = \max[0, \min(1, \Theta)]. \tag{3.8}$$

For simplicity, only the formulae for $c_{\alpha y} > 0$ and $c_{\alpha x} > 0$ are given.

3.2. *Boundary condition*

Gas–wall interactions are captured by boundary conditions. The most popular boundary condition is the Maxwell model (Clerk Maxwell 1879; Cercignani 2000),

https://doi.org/10.1017/jfm.2012.616 Published online by Cambridge University Press

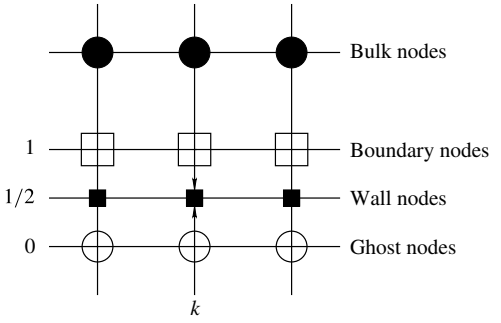


FIGURE 2. Schematic illustration of wall boundary treatment.

in which a fraction $(1-\gamma)$ of gas particles are assumed to undergo specular reflection while the remaining particles are diffusely reflected. In the limit of $\gamma = 1$, the reflection becomes fully diffuse.

As lattice models are derived from continuous kinetic equations, their boundary conditions may be obtained from the continuous kinetic theory (Ansumali & Karlin 2002). It has already been shown that lattice models with a diffuse-type wall boundary can describe a range of rarefaction effects (see e.g. Kim *et al.* 2008*a*; Yudistiawan *et al.* 2008; Meng & Zhang 2011*b*). In this work, our primary interest is the model accuracy; as a result we will only implement the Maxwellian diffuse wall boundary.

The boundary condition employed in this work is Version 1 of boundary conditions in Sofonea (2009), which is briefly described below. Firstly, the truncated Maxwellian distribution function can be written as

$$\begin{aligned} f_\alpha^{(0)} &= \rho S(T, \boldsymbol{u}) \\ &= \rho w_\alpha \left\{ 1 + c_i u_i + \frac{1}{2}\left[(c_i u_i)^2 - u_i u_i + (T-1)(c_i c_i - D)\right] \right. \\ &\quad + \frac{c_i u_i}{6}\left[(c_i u_i)^2 - 3u_i u_i + 3(T-1)(c_i c_i - D - 2)\right] \\ &\quad + \frac{1}{24}\left[(c_i u_i)^4 - 6\,(u_i c_i)^2\, u_j u_j + 3\,(u_j u_j)^2\right] \\ &\quad + \frac{T-1}{4}\left[(c_i c_i - D - 2)((u_i c_i)^2 - u_i u_i) - 2\,(u_i c_i)^2\right] \\ &\quad \left. + \frac{(T-1)^2}{8}\left[(c_i c_i)^2 - 2(D+2)c_i c_i + D(D+2)\right] \right\}. \end{aligned} \tag{3.9}$$

As the discretization is conducted along a Cartesian coordinate system (see figure 2), the wall boundary condition can be written as

$$f_{\alpha,k}^0 = \rho_{W,k} S(T_{W,k}, \boldsymbol{u}_{W,k}), \quad \boldsymbol{c}_\alpha \cdot \boldsymbol{n} > 0, \tag{3.10}$$

where

$$\rho_{W,k} = \frac{\displaystyle\sum_{(\boldsymbol{c}_\alpha \cdot \boldsymbol{n})<0} |\boldsymbol{c}_\alpha \cdot \boldsymbol{n}| f_{\alpha,k}^1}{\displaystyle\sum_{(\boldsymbol{c}_\alpha \cdot \boldsymbol{n})>0} |\boldsymbol{c}_\alpha \cdot \boldsymbol{n}| S(T_{W,k}, \boldsymbol{u}_{W,k})}. \tag{3.11}$$

https://doi.org/10.1017/jfm.2012.616 Published online by Cambridge University Press

Here, the superscripts 0 and 1 represent the ghost and boundary nodes, respectively, subscript W denotes the computational nodes at the wall, $\rho_{W,k}$ is the density on the wall nodes k (see figure 2), $T_{W,k}$ is the temperature, $\boldsymbol{u}_{W,k}$ the velocity and $\boldsymbol{n}$ the inward unit vector normal to the wall. The distribution function at the ghost nodes is assumed to be identical to those on the corresponding wall nodes.

4. Validation

We have validated the proposed scheme using a variety of flows, both in the low- and high-Mach-number limit. Unless otherwise stated, our results have been obtained using an 11th-order discrete velocity set, which represents a good compromise between accuracy (expected to be accurate at the Burnett level, see § 2.3) and computational efficiency. Our numerical results will be compared with direct and low-variance deviational Monte Carlo (DSMC and LVDSMC) (see Homolle & Hadjiconstantinou 2007; Radtke & Hadjiconstantinou 2009; Radtke, Hadjiconstantinou & Wagner 2011) simulations, while in some cases, numerical solutions of the ES-BGK equation and analytical results of the R13 model will also be presented.

The flows considered here are one-dimensional and are confined by two infinite parallel plates in the x–z plane. The distance between the two plates (in the y direction) is L on which the Knudsen number

$$K_D = \sqrt{\frac{\pi}{2}} Kn \tag{4.1}$$

is based. Comparisons with the hard-sphere gas will be performed by setting the Prandtl number to 2/3, i.e. $b = -1/2$. For the BGK gas, the Prandtl number is unity which corresponds to $b = 0$. Furthermore, the gas has the heat capacity $C_p = 5/2$, i.e. the spatial dimension D is set to be 3, see (2.3) and (3.9). Our simulation results ($D = 3$) are described below.

4.1. *Low-Mach-number flows*

Flows in the low-Mach-number limit are of particular interest since they are most often encountered in micro/nanofluidic applications (Cercignani 2006; Hadjiconstantinou 2006). Here we provide validation of our methodology using traditional Couette and Fourier flows. We also present solutions of an unsteady boundary heating problem that features coupled momentum and heat transfer and thus requires an accurate representation of the ratio of the associated transport coefficients, namely the Prandtl number. This problem also allows us to investigate the limitations of the proposed model in the presence of kinetic effects due to flow unsteadiness.

4.1.1. *Steady Couette and Fourier flows*

Figures 3 and 4 show comparison between our lattice results and DSMC simulations for a Couette and a Fourier heat transfer problem respectively. In the Couette flows, the walls move with velocities $u_w = \pm 0.1$, while in the Fourier problems the wall temperatures are $T_w = 1 \pm 0.05$. Figure 4 shows that the proposed lattice ES-BGK model can be used to approximate the hard-sphere gas thermal conduction by setting the Prandtl number to 2/3. Both figures show that the agreement in the slip-flow regime is excellent; as K_D increases into the transition regime, a small amount of error is evident. This error increases further as K_D increases, but remains very reasonable for $K_D < 0.5$; for example, for both flows, at $K_D = 0.5$ the error is less than 5 %.

https://doi.org/10.1017/jfm.2012.616 Published online by Cambridge University Press

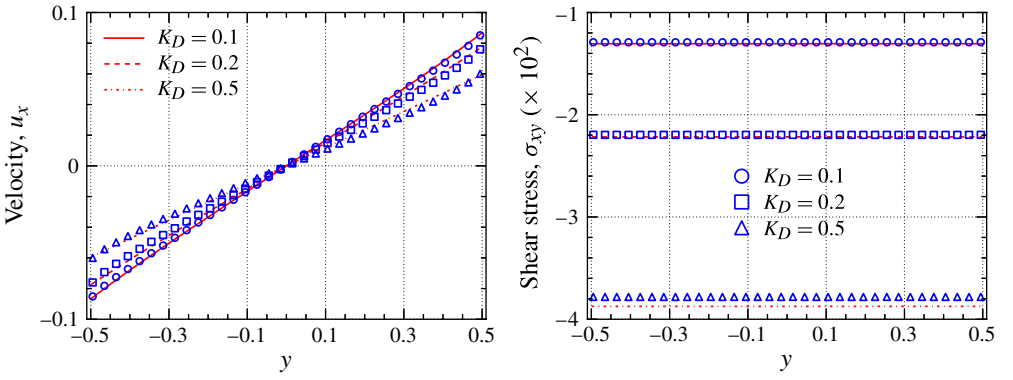


FIGURE 3. (Colour online) The velocity and shear stress profiles for Couette flow of a hard-sphere gas at $K_D = 0.1$, 0.2 and 0.5. The symbols denote DSMC data and the lines represent the lattice ES-BGK results. The wall velocities are $u_w = \pm 0.1$.

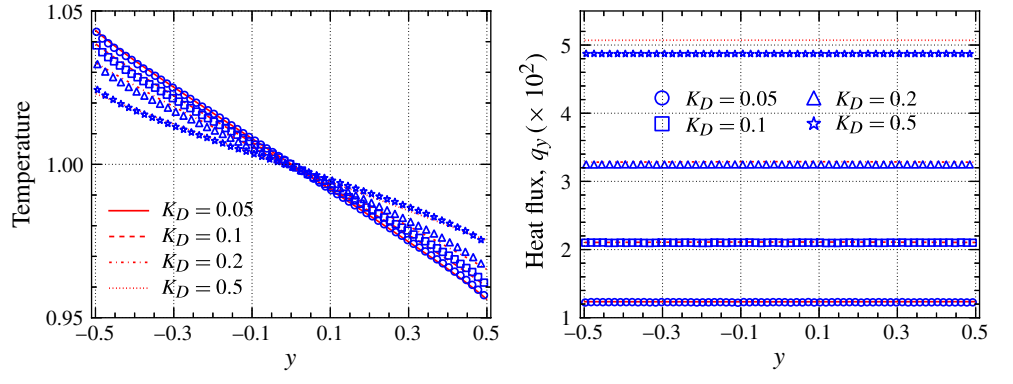


FIGURE 4. (Colour online) The temperature and heat flux profiles for a Fourier problem for a hard-sphere gas at $K_D = 0.05$, 0.1, 0.2 and 0.5 with the wall temperature difference 0.1. The symbols denote DSMC data and the lines represent the lattice ES-BGK results.

4.1.2. *Unsteady boundary heating problems*

In this section we present results from an unsteady boundary heating problem of the kind studied in Manela & Hadjiconstantinou (2007); these studies are motivated by the common occurrence of applications involving time-varying boundary temperatures in micro-electro-mechanical devices. In this problem, the two walls confining the gas are heated uniformly via prescribed time-dependent temperatures of the form $T_w = 1 + F(t)$. Here, $F(t)$ is taken to be a sinusoidal function $\sin(\theta t)$ with an amplitude (0.002 in simulations) that is sufficiently small to justify a linear assumption. As this is a time-varying problem, another non-dimensional parameter needs to be introduced (Manela & Hadjiconstantinou 2008, 2010), namely the Strouhal number, defined as

$$St = \theta = \frac{\hat{\theta} L}{\sqrt{R T_0}}. \tag{4.2}$$

https://doi.org/10.1017/jfm.2012.616 Published online by Cambridge University Press

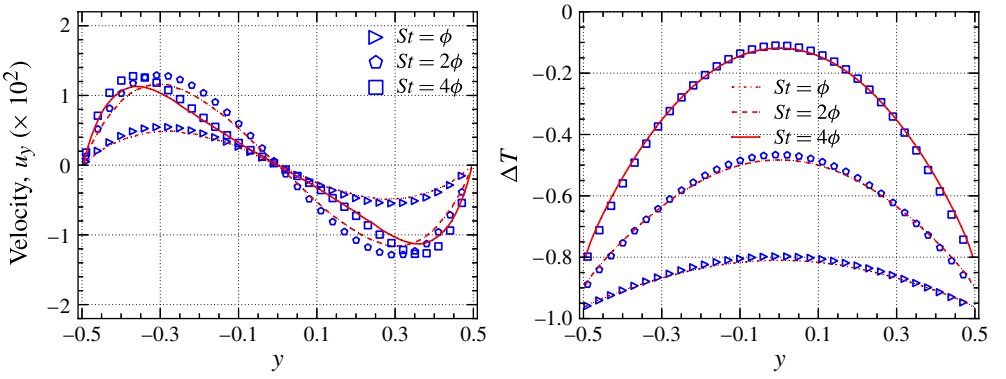


FIGURE 5. (Colour online) The velocity and temperature perturbations for a hard-sphere gas subject to a sinusoidal heating at $t = 3\pi/2$ at $K_E = 0.05$ and different St, where $\phi = \pi\sqrt{2}/16$. The symbols correspond to the data of the lattice model ($Pr = 2/3$) and the lines are the results of the LVDSMC method.

Kinetic effects become important as both the Strouhal and Knudsen numbers increase as shown in figure 6 in Manela & Hadjiconstantinou (2010).

Here, simulations will be conducted for a range of Strouhal and Knudsen numbers. Prandtl numbers corresponding both to the hard-sphere and BGK model will be considered. The accuracy of the lattice results will be evaluated by comparison with simulation results obtained using the recently developed low-variance deviational simulation Monte Carlo (LVDSMC) method (Homolle & Hadjiconstantinou 2007; Radtke & Hadjiconstantinou 2009; Radtke *et al.* 2011) because simulation of this low-Mach-number flow by DSMC is prohibitively expensive. The LVDSMC method was developed to specifically address this DSMC limitation, namely the prohibitive computational cost associated with low-*Ma* and more generally low-signal flows. LVDSMC provides efficient numerical solutions of the Boltzmann equation for all Knudsen numbers (Wagner 2008) and arbitrarily small signals by simulating only the deviation from equilibrium. This control-variate variance-reduction formulation introduces deterministic knowledge of a nearby equilibrium state, and thus significantly reduces the statistical uncertainty associated with the Monte Carlo approach without introducing any approximation. The resulting computational benefits in the limit of low-speed flows such as the one considered here are typically very large (Homolle & Hadjiconstantinou 2007).

Following Manela & Hadjiconstantinou (2010), comparison with LVDSMC results will be performed using the following two Knudsen numbers:

$$K_E = \frac{16}{5\sqrt{2\pi}} Kn, \tag{4.3}$$

for the hard-sphere gas with $Pr = 2/3$, and

$$K_B = \sqrt{\frac{8}{\pi}} Kn \tag{4.4}$$

for the BGK gas with $Pr = 1$. Details on the LVDSMC simulations of the problem studied here can be found in Manela & Hadjiconstantinou (2008, 2010).

https://doi.org/10.1017/jfm.2012.616 Published online by Cambridge University Press

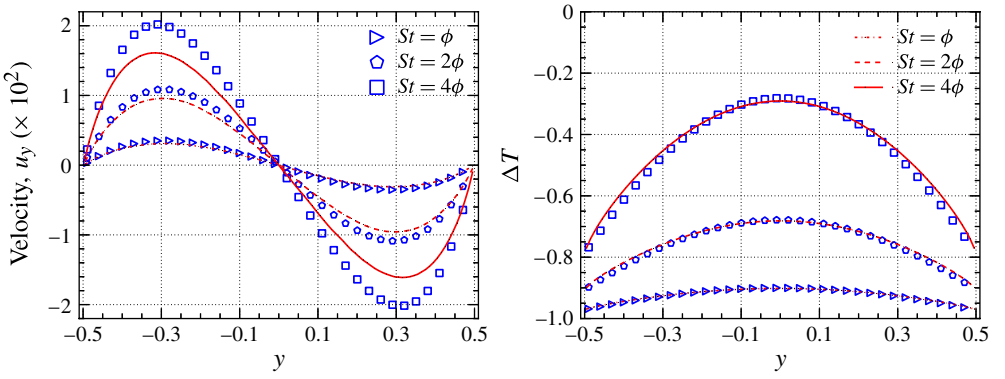


FIGURE 6. (Colour online) The velocity and temperature perturbations (ΔT) for a hard-sphere gas subject to a sinusoidal heating at $t = 3\pi/2$ at $K_E = 0.1$ and different St where $\phi = \pi\sqrt{2}/16$. The symbols correspond to the data of the lattice model ($Pr = 2/3$) and the lines are the results of the LVDSMC method.

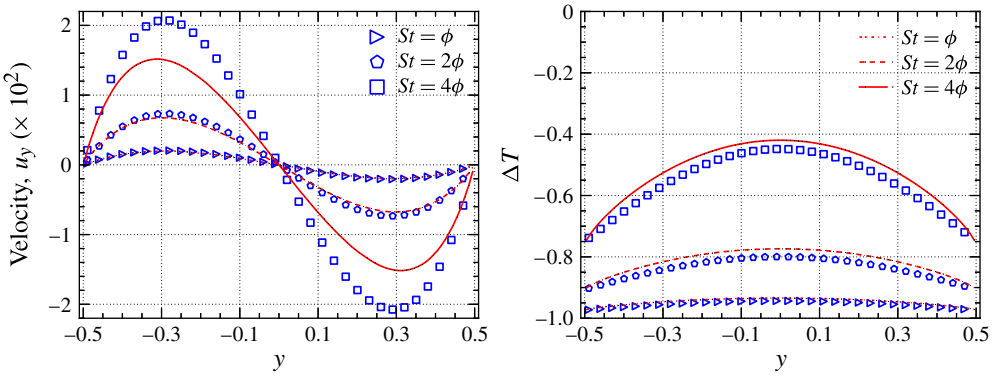


FIGURE 7. (Colour online) The velocity and temperature perturbations for a hard-sphere gas subject to a sinusoidal heating at $t = 3\pi/2$ at $K_E = 0.2$ and different St where $\phi = \pi\sqrt{2}/16$. The symbols correspond to the data of the lattice model ($Pr = 2/3$) and the lines are the results of the LVDSMC method.

The results for various Strouhal and Knudsen numbers for the hard-sphere model are presented in figures 5–8, where both the velocity u_y and temperature perturbation $\Delta T = T - 1$ are normalized by the amplitude of $F(t)$. Figures 9–12 show results for the BGK model. Symbols denote the lattice model proposed here, whereas lines denote LVDSMC data. At $St = \pi\sqrt{2}/16$, the two sets of results show good agreement, even when $K_E = 0.5$ or $K_B = 0.5$. With increasing Strouhal number, discrepancies between the two appear and become larger. For $St = \pi\sqrt{2}/4$, significant disagreement is observed even for K_E as low as 0.05. Larger Strouhal numbers lead to stronger rarefaction effects, so this disagreement can be attributed to the moderate discrete velocity set. Overall, with this moderate discrete velocity set, the present model can give reasonable predictions for flows with a Knudsen number up to 0.5 and a Strouhal number up to $\pi\sqrt{2}/8$. If highly accurate results are desirable, more discrete velocities are required, leading to higher computational costs.

https://doi.org/10.1017/jfm.2012.616 Published online by Cambridge University Press

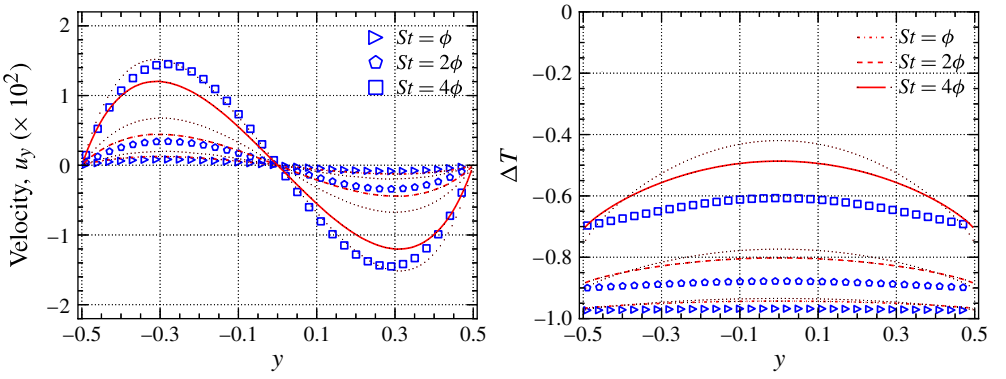


FIGURE 8. (Colour online) The velocity and temperature perturbations for a hard-sphere gas subject to a sinusoidal heating at $t = 3\pi/2$ at $K_E = 0.5$ and different St where $\phi = \pi\sqrt{2}/16$. The symbols correspond to the data of the lattice model ($Pr = 2/3$) and the lines are the results of the LVDSMC method.

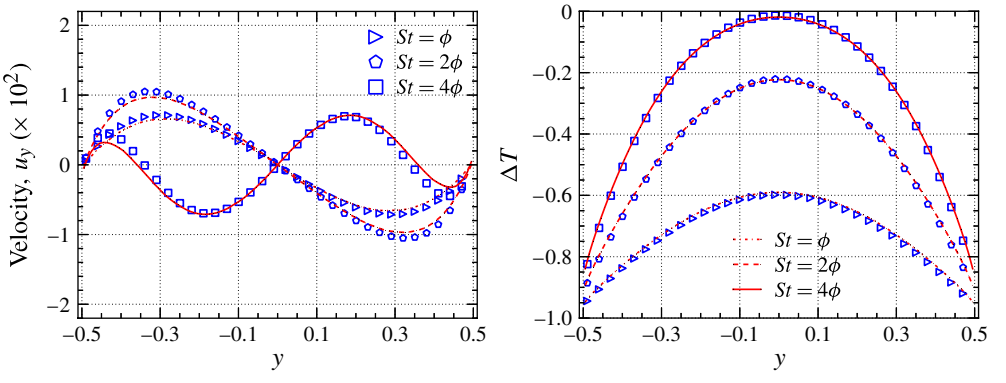


FIGURE 9. (Colour online) The velocity and temperature perturbations for a BGK gas subject to a sinusoidal heating at $t = 3\pi/2$ at $K_B = 0.05$ and different St where $\phi = \pi\sqrt{2}/16$. The symbols correspond to the data of the lattice model ($Pr = 1$) and the lines are the results of the LVDSMC method.

4.2. *High-Mach-number flows*

In this section we present simulation results for high-Mach-number flows such as Couette flows with $u_w = \pm 0.2$ and forced Poiseuille flows with non-dimensional forcing magnitude $g = 0.22$. Although in the Couette flows the wall speed is only a factor of 2 larger than the flows examined in § 4.1, our focus here turns to the resulting temperature field that, despite the small temperature differences involved, reveals useful information.

Figure 13 shows a comparison between our lattice model, DSMC and numerical solution of the ES-BGK equation for a Couette flow at $K_D = 0.05$. The comparison reveals that at these small K_D, the lattice model can capture both kinetic (e.g. velocity slip/temperature jump) and non-equilibrium effects quite accurately. For comparison, the results of the BGK equation and its lattice version ($b = 0$) are also presented.

https://doi.org/10.1017/jfm.2012.616 Published online by Cambridge University Press

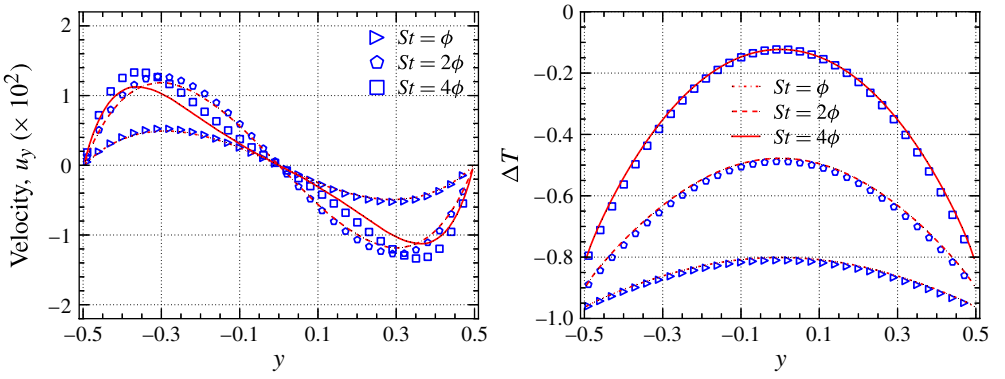


FIGURE 10. (Colour online) The velocity and temperature perturbations (ΔT) for a BGK gas subject to a sinusoidal heating at $t = 3\pi/2$ at $K_B = 0.1$ and different St where $\phi = \pi\sqrt{2}/16$. The symbols correspond to the data of the lattice model ($Pr = 1$) and the lines are the results of the LVDSMC method.

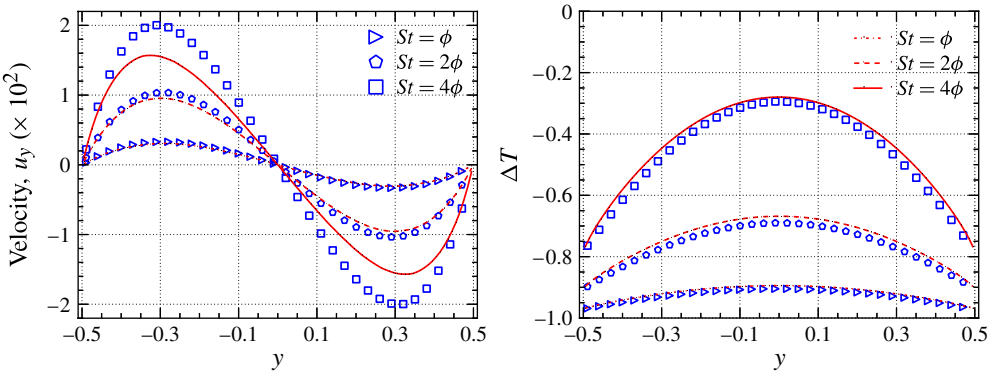


FIGURE 11. (Colour online) The velocity and temperature perturbations for a BGK gas subject to a sinusoidal heating at $t = 3\pi/2$ at $K_B = 0.2$ and different St where $\phi = \pi\sqrt{2}/16$. The symbols correspond to the data of the lattice model ($Pr = 1$) and the lines are the results of the LVDSMC method.

These two models predict a temperature maximum that is 30 % higher than the hard-sphere result.

Results for Couette flows in the transition regime are presented in figures 14 and 15. Overall, our model predictions for the velocity, shear stress and heat flux are close to those of DSMC even for $K_D = 0.5$. However, our predictions of the viscous-heating-induced temperature field start to deviate from the DSMC results at $K_D = 0.2$. Remarkably, the heat flux predictions of the lattice model are still in excellent agreement with the DSMC data for K_D as large as 0.5.

To further validate the model accuracy beyond the NS level, the profiles of shear stress σ_{yy} and streamwise heat flux q_x are presented in figure 16, which are both zero at the NS level of approximation. However, our lattice model can give reasonable predictions for σ_{yy} up to $K_D = 0.2$ which is consistent with the temperature prediction. For the heat flux q_x, we can make a similar observation, which further confirms

https://doi.org/10.1017/jfm.2012.616 Published online by Cambridge University Press

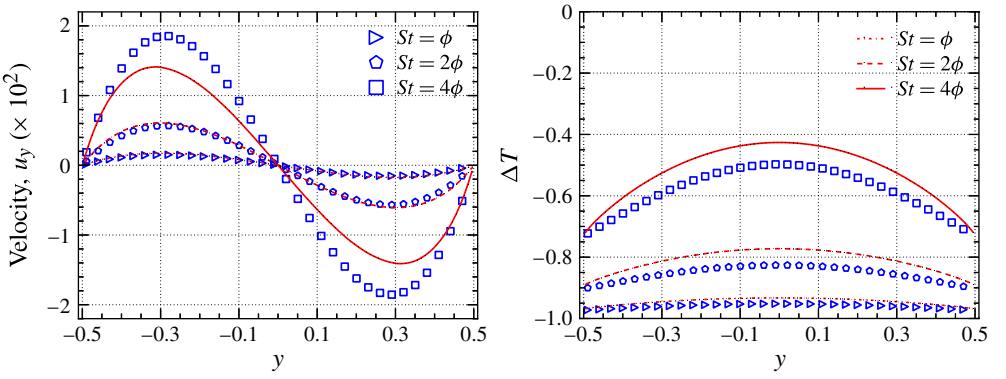


FIGURE 12. (Colour online) The velocity and temperature perturbations for a BGK gas subject to a sinusoidal heating at $t = 3\pi/2$ at $K_B = 0.5$ and different St where $\phi = \pi\sqrt{2}/16$. The symbols correspond to the data of the lattice model ($Pr = 1$) and the lines are the results of the LVDSMC method.

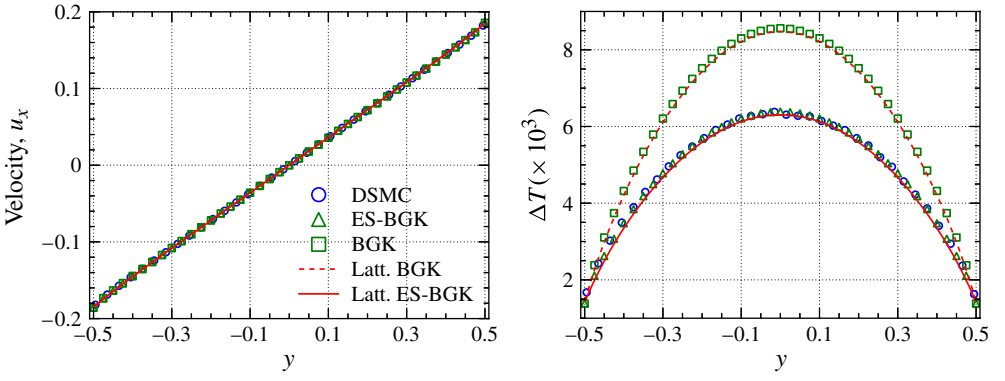


FIGURE 13. (Colour online) The velocity and temperature profiles for the Couette flow at $K_D = 0.05$, where $\Delta T = T - T_w$. The wall velocities are $u_w = \pm 0.2$.

that our model can describe kinetic effects beyond the NS level with the chosen moderate 11th-order quadrature, which is consistent with the discussion in § 2.3. It is also interesting to compare with the predictions of the R13 model, which is supposed to give a stable set of transport equations of the super-Burnett order (Taheri *et al.* 2009). Figure 16 shows that the R13 model and our lattice model give similar results.

The simulation results for Poiseuille flows at four Knudsen numbers are depicted in figures 17 and 18. This flow is more numerically challenging compared to the Couette flow. Even for K_D as small as 0.1, the temperature profiles show significant difference between the lattice model and DSMC results, even though the bimodal temperature distribution (Mansour, Baras & Garcia 1997) can be qualitatively captured by the lattice model at $K_D = 0.2$. As the Knudsen number increases further, the difference becomes even larger, though the temperature minimum at the centre of the computational domain can be predicted qualitatively. Remarkably, but also consistently with the Couette flow case, the heat flux profiles show good agreement with the DSMC data despite the more significant discrepancies in the temperature profiles.

https://doi.org/10.1017/jfm.2012.616 Published online by Cambridge University Press

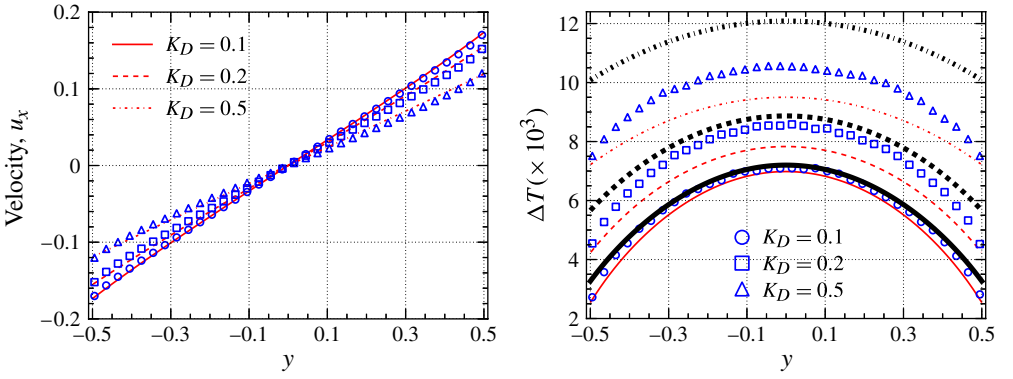


FIGURE 14. (Colour online) The velocity and temperature profiles ($\Delta T = T - T_w$) for Couette flow of a hard-sphere gas at $K_D = 0.1$, 0.2 and 0.5. The symbols denote the DSMC data and the thin lines (red online) represent the lattice ES-BGK results. The wall velocities are $u_w = \pm 0.2$. For further comparison, the temperature profiles predicted by the R13 model (Taheri *et al.* 2009) are also presented with thick black lines, where the line styles for the different Knudsen numbers are the same as those for the lattice ES-BGK results.

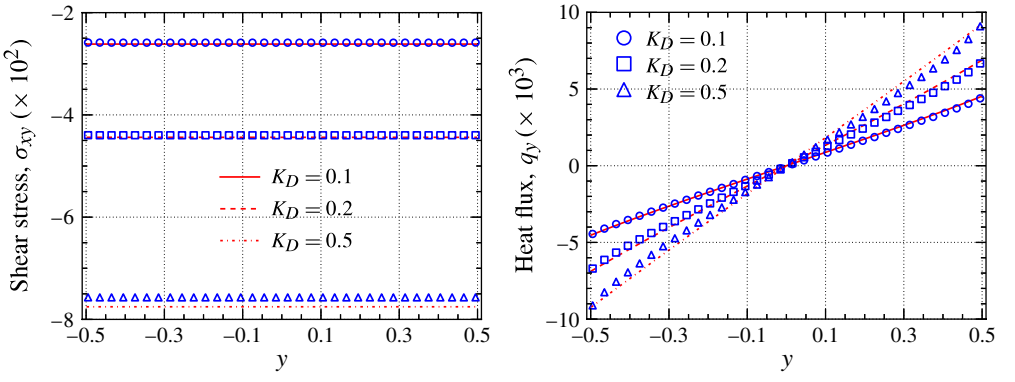


FIGURE 15. (Colour online) The shear stress (σ_{xy}) and heat flux (q_y) profiles for Couette flow of a hard-sphere gas at $K_D = 0.1$, 0.2 and 0.5. The symbols denote DSMC data and the lines represent the lattice ES-BGK results. The wall velocities are $u_w = \pm 0.2$.

The inability of our model to predict accurate viscous heating may be caused by two factors. First, as shown in the derivation process, the lattice model approaches the corresponding kinetic model via the moment representation with increasing order of Gauss–Hermite quadrature. However, as discussed in § 2.3, the chosen moderate discrete velocity set is only expected to approach the Burnett level, which may not be sufficient to capture all kinetic effects in the presence of a non-negligible Mach number. This is verified in figure 19 where its is shown that enriching the discrete velocity set can improve the model accuracy.

In addition to the error due to a finite number of discrete velocities, the ES-BGK equation itself is a model which may be failing in these flows. In fact, as shown by some studies (e.g. Gallis & Torczynski 2011), the ES-BGK equation tends to produce

https://doi.org/10.1017/jfm.2012.616 Published online by Cambridge University Press

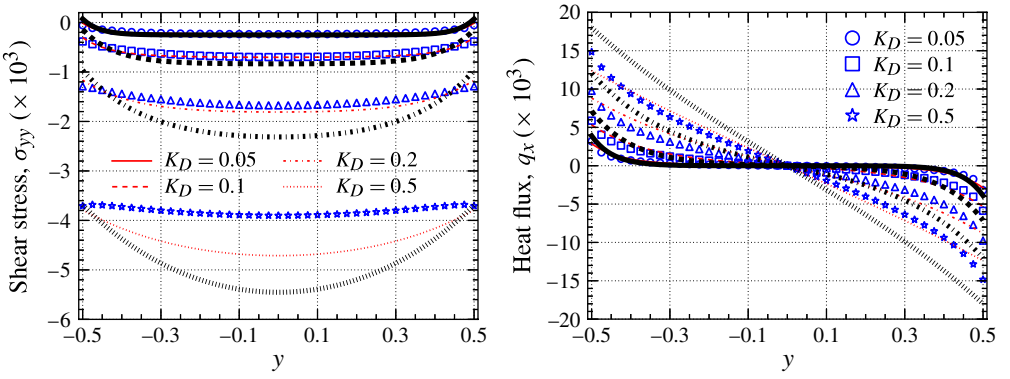


FIGURE 16. (Colour online) The shear stress (σ_{yy}) and heat flux (q_x) profiles for Couette flow of a hard-sphere gas at $K_D = 0.05, 0.1, 0.2$ and 0.5. The symbols denote direct solution of the ES-BGK equation, the thin lines (red online) represent the lattice ES-BGK results and the thick black lines are those of the R13 model (Taheri *et al.* 2009). The Knudsen numbers for the R13 model are denoted using the same line styles as the lattice ES-BGK results. The wall velocities are $u_w = \pm 0.2$.

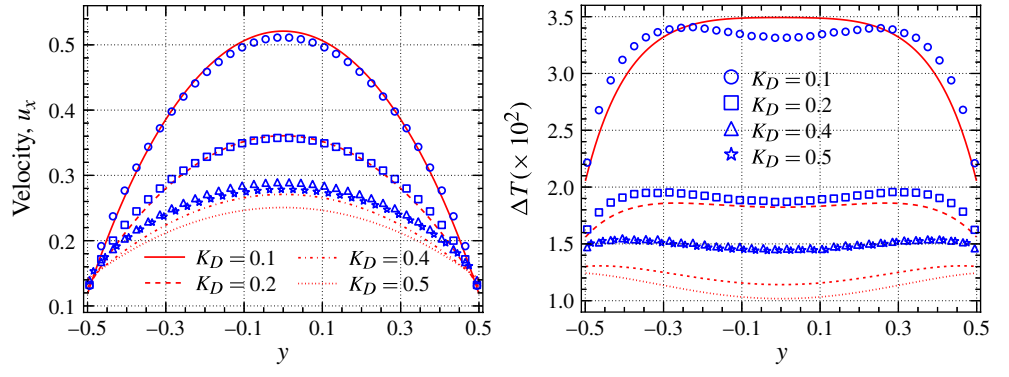


FIGURE 17. (Colour online) The velocity and temperature profiles ($\Delta T = T - T_w$) for the force-driven Poiseuille flow of a hard-sphere gas at $K_D = 0.1, 0.2, 0.4$ and 0.5. The symbols denote DSMC data and the lines represent the lattice ES-BGK results.

inaccurate velocity distribution functions. The possibility that the ES-BGK model is itself contributing to the error can be confirmed by the results presented in figure 20. At $K_D = 0.5$ the lattice model result shows a significant deviation from the numerical solution of the ES-BGK model. Meanwhile, the temperature profile from numerical solution of the ES-BGK equation itself shows a large deviation from the DSMC result.

While the comparisons with the DSMC solutions for the temperature difference of 0.1 have been shown in figure 4, a larger temperature difference of 0.3 was investigated for the combined Couette–Fourier flow. The results are shown in figure 21 where excellent agreement is observed between the lattice ES-BGK model and the ES-BGK equation.

https://doi.org/10.1017/jfm.2012.616 Published online by Cambridge University Press

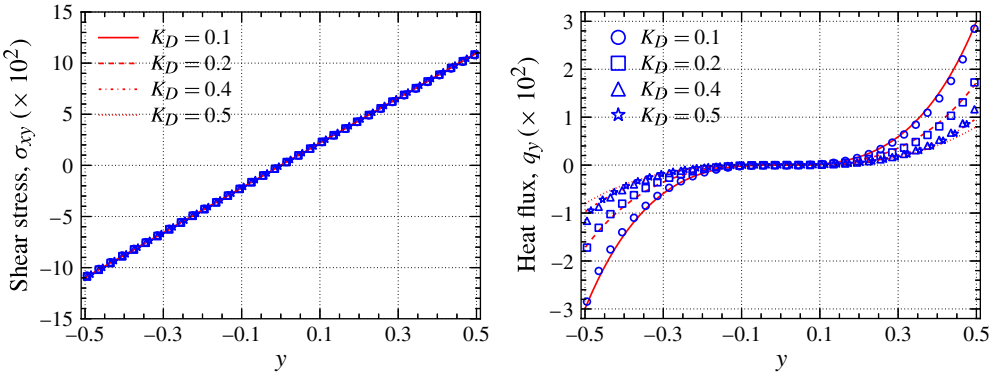


FIGURE 18. (Colour online) The shear stress and heat flux profiles for the force-driven Poiseuille flow of a hard-sphere gas at $K_D = 0.1$, 0.2, 0.4 and 0.5. The symbols denote DSMC data and the lines represent the lattice ES-BGK results.

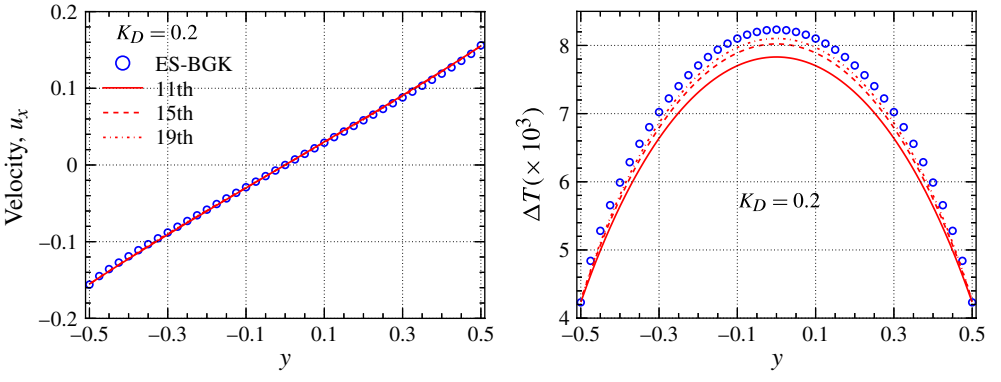


FIGURE 19. (Colour online) Convergence comparison for a Couette flow at $K_D = 0.2$ with wall velocities $u_w = \pm 0.2$. Lines denote the lattice model data, and the adopted discrete velocity order as denoted in the legend. Improved accuracy is observed as the number of discrete velocities is increased.

5. Concluding remarks

We have presented and validated a lattice Boltzmann model using a systematic Hermite moment representation of the ES-BGK equation. The resulting lattice ES-BGK model features an adjustable Prandtl number and may thus be more appropriate for use in coupled thermofluidic phenomena. This generic procedure may be applied to other kinetic model equations.

We have validated the lattice model for combined thermal and rarefaction effects by comparing its predictions with DSMC and LVDSMC results as well as numerical solutions of the ES-BGK model. We find that, for a moderate 11th-order discrete velocity set, the proposed model can provide reasonable predictions for Couette and force-driven Poiseuille flows for Knudsen numbers up to 0.5. In addition, it is able to accurately predict heat conduction in the slip-flow and early transition regimes. This

https://doi.org/10.1017/jfm.2012.616 Published online by Cambridge University Press

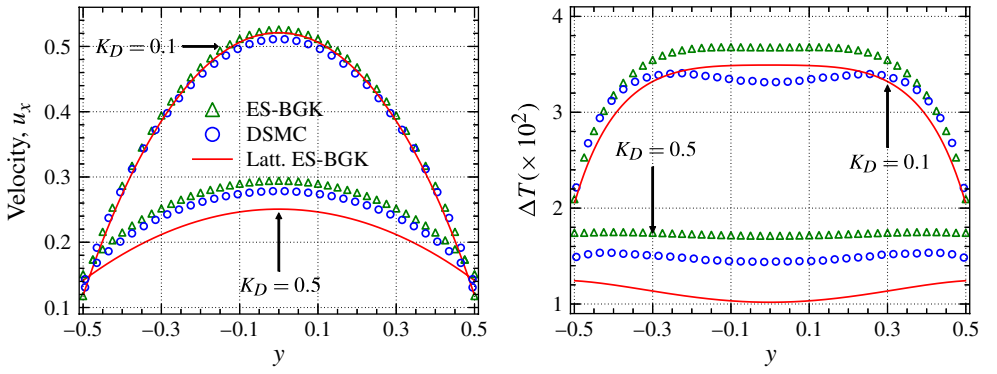


FIGURE 20. (Colour online) Comparisons of the velocity and temperature profiles ($\Delta T = T - T_w$) for the force-driven flow among the ES-BGK equation, lattice ES-BGK model and DSMC method at $K_D = 0.1$ and 0.5.

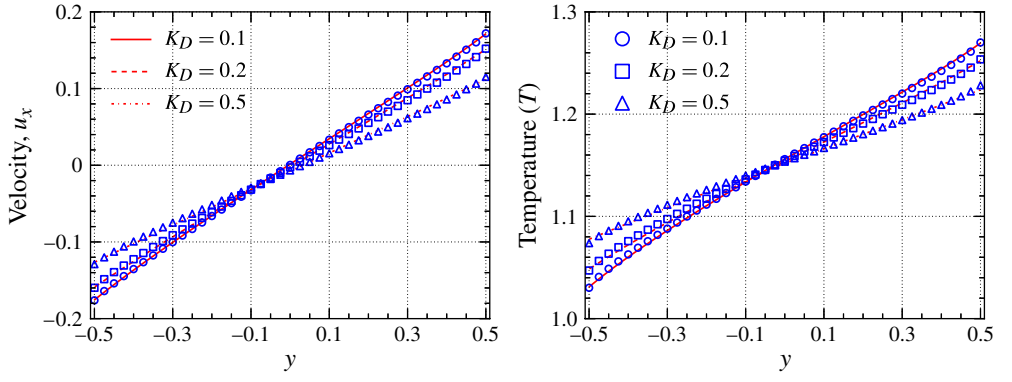


FIGURE 21. (Colour online) Comparisons of the velocity and temperature profiles for the combined Couette–Fourier flows. The wall velocities are $u_w = \pm 0.2$ while the wall temperature difference is 0.3. The lines are the lattice ES-BGK model data and the symbols are the results of the ES-BGK equation.

finding extends to unsteady problems provided the additional kinetic effects due to their time-dependence are also considered: for an unsteady boundary heating problem reasonable agreement with LVDSMC simulations is observed for Knudsen numbers up to 0.5 and Strouhal numbers up to $\pi\sqrt{2}/8$.

The solutions obtained by the lattice Boltzmann method are expected to approach the 'true' solutions of the ES-BGK equation as the number of discrete velocities and the Hermite expansion order is increased. However, the moderate discrete velocity set used here already represents a reasonable compromise between computational efficiency and modelling accuracy for flows with a range of Knudsen and Strouhal numbers. Although we have tested the model for rarefied-gas thermal flows, this model, in principle, can be used for liquid thermal flows, which will be the subject of future work.

https://doi.org/10.1017/jfm.2012.616 Published online by Cambridge University Press

REFERENCES

ANDRIES, P., BOURGAT, J.-F., LE TALLEC, P. & PERTHAME, B. 2002 Numerical comparison between the Boltzmann and ES-BGK models for rarefied gases. *Comput. Meth. Appl. Mech. Engng* **191** (31), 3369–3390.

ANDRIES, P., TALLEC, P. LE., PERLAT, J.-P. & PERTHAME, B. 2000 The Gaussian-BGK model of Boltzmann equation with small Prandtl numbe. *Eur. J. Mech.* (B/*Fluids*) **19** (6), 813–830.

ANSUMALI, S. & KARLIN, I. V. 2002 Kinetic boundary conditions in the lattice Boltzmann method. *Phys. Rev.* E **66** (2), 26311.

ANSUMALI, S., KARLIN, I. V., ARCIDIACONO, S., ABBAS, A. & PRASIANAKIS, N. I. 2007 Hydrodynamics beyond Navier–Stokes: exact solution to the lattice Boltzmann hierarchy. *Phys. Rev. Lett.* **98** (12), 124502.

AOKI, K., TAKATA, S. & NAKANISHI, T. 2002 Poiseuille-type flow of a rarefied gas between two parallel plates driven by a uniform external force. *Phys. Rev.* E **65** (2), 26315.

CERCIGNANI, C. 2000 *Rarefied Gas Dynamics: From Basic Concepts to Actual Calculations*. Cambridge University Press.

CERCIGNANI, C. 2006 *Slow Rarefied Flows: Theory and Application to Micro-Electro-Mechanical Systems*. Birkhauser.

CHEN, S. Y. & DOOLEN, G. D. 1998 Lattice Boltzmann method for fluid flows. *Annu. Rev. Fluid Mech.* **30**, 329–364.

CHIKATAMARLA, S. S. & KARLIN, I. V. 2006 Entropy and Galilean invariance of lattice Boltzmann theories. *Phys. Rev. Lett.* **97** (19), 190601.

CHIKATAMARLA, S. S. & KARLIN, I. V. 2009 Lattices for the lattice Boltzmann method. *Phys. Rev.* E **79** (4), 46701.

CLERK MAXWELL, J. 1879 On stresses in rarified gases arising from inequalities of temperature. *Phil. Trans. R. Soc. Lond.* **170**, 231–256.

GALLIS, M. A. & TORCZYNSKI, J. R. 2011 Investigation of the ellipsoidal-statistical Bhatnagar–Gross–Brook kinetic model applied to gas-phase transport of heat and tangential momentum between parallel walls. *Phys. Fluids* **23** (3), 030601.

GARZÓ, V. & SANTOS, A. 1995 Comparison between the Boltzmann and BGK equations for uniform shear flow. *Physica* A **213**, 426–434.

GONNELLA, G., LAMURA, A. & SOFONEA, V. 2007 Lattice Boltzmann simulation of thermal nonideal fluids. *Phys. Rev.* E **76** (3), 36703.

GRAD, H. 1949 On the kinetic theory of rarefied gases. *Commun. Pure Appl. Maths* **2**, 331–407.

GRAD, H. 1958 *Principles of the Kinetic Theory of Gases*, Handbuch der Physik XII: Thermodynamik der Gase Edn. Springer.

GRAUR, I. & POLIKARPOV, A. 2009 Comparison of different kinetic models for the heat transfer problem. *Heat Mass Transfer* **46** (2), 237–244.

GU, X. J. & EMERSON, D. R. 2007 A computational strategy for the regularized 13 moment equations with enhanced wall-boundary conditions. *J. Comput. Phys.* **225** (1), 263–283.

GU, X.-J. & EMERSON, D. R 2009 A high-order moment approach for capturing non-equilibrium phenomena in the transition regime. *J. Fluid Mech.* **636**, 177–216.

GUO, Z., ZHAO, T. S. & SHI, Y. 2006 Physical symmetry, spatial accuracy, and relaxation time of the lattice Boltzmann equation for microgas flows. *J. Appl. Phys.* **99** (7), 74903.

GUO, Z., ZHENG, C., SHI, B. & ZHAO, T. S. 2007 Thermal lattice Boltzmann equation for low Mach number flows: decoupling model. *Phys. Rev.* E **75** (3), 36704.

HADJICONSTANTINOU, N. G. 2006 The limits of Navier–Stokes theory and kinetic extensions for describing small-scale gaseous hydrodynamics. *Phys. Fluids* **18** (11), 111301.

HAN, Y.-L., MUNTZ, E. P. & ALEXEENKO, A. 2011 Nanoscale and microscale thermophysical engineering experimental and computational studies of temperature gradient–driven molecular transport in gas flows through nano/microscale Channels. *Nanoscale Microscale Thermophys. Engng* 37–41.

HAN, Y.-L., MUNTZ, E. P., ALEXEENKO, A. & YOUNG, M. 2007 Experimental and computational studies of temperature gradient-driven molecular transport in gas flows through nano/microscale channels. *Nanoscale Microscale Thermophys. Engng* **11** (1–2), 151–175.

https://doi.org/10.1017/jfm.2012.616 Published online by Cambridge University Press

HE, X., CHEN, S. & DOOLEN, G. D 1998 A novel thermal model for the lattice Boltzmann method in incompressible limit. *J. Comput. Phys.* **146** (1), 282–300.

HOLWAY, L. H. 1966 New statistical models for kinetic theory: methods of construction. *Phys. Fluids* **9** (9), 1658–1673.

HOMOLLE, T. M. M. & HADJICONSTANTINOU, N. G. 2007 A low-variance deviational simulation Monte Carlo for the Boltzmann equation. *J. Comput. Phys.* **226** (2), 2341–2358.

KIM, S. H., PITSCH, H. & BOYD, I. D. 2008*a* Accuracy of higher-order lattice Boltzmann methods for microscale flows with finite Knudsen numbers. *J. Comput. Phys.* **227** (19), 8655–8671.

KIM, S. H., PITSCH, H. & BOYD, I. D. 2008*b* Slip velocity and Knudsen layer in the lattice Boltzmann method for microscale flows. *Phys. Rev.* E **77** (4), 26704.

LALLEMAND, P. & LUO, L.-S. 2003 Theory of the lattice Boltzmann method: acoustic and thermal properties in two and three dimensions. *Phys. Rev.* E **68** (3), 36706.

MANELA, A. & HADJICONSTANTINOU, N. G. 2007 On the motion induced in a gas confined in a small-scale gap due to instantaneous heating. *J. Fluid Mech.* **593**, 453–462.

MANELA, A. & HADJICONSTANTINOU, N. G. 2008 Gas motion induced by unsteady boundary heating in a small-scale slab. *Phys. Fluids* **20** (11), 117104.

MANELA, A. & HADJICONSTANTINOU, N. G. 2010 Gas-flow animation by unsteady heating in a microchannel. *Phys. Fluids* **22** (6), 62001.

MANSOUR, M. M., BARAS, F. & GARCIA, A. L. 1997 On the validity of hydrodynamics in plane Poiseuille flows. *Physica* A **240** (1–2), 255–267.

MENG, J. & ZHANG, Y. 2011*a* Accuracy analysis of high-order lattice Boltzmann models for rarefied gas flows. *J. Comput. Phys.* **230** (3), 835–849.

MENG, J. & ZHANG, Y. 2011*b* Gauss–Hermite quadratures and accuracy of lattice Boltzmann models for nonequilibrium gas flows. *Phys. Rev.* E **83** (3).

MIEUSSENS, L. & STRUCHTRUP, H. 2004 Numerical comparison of Bhatnagar–Gross–Krook models with proper Prandtl number. *Phys. Fluids* **16** (8), 2797–2813.

PRASIANAKIS, N. I. & KARLIN, I. V. 2007 Lattice Boltzmann method for thermal flow simulation on standard lattices. *Phys. Rev.* E **76** (1), 16702.

PRASIANAKIS, N. I. & KARLIN, I. V. 2008 Lattice Boltzmann method for simulation of compressible flows on standard lattices. *Phys. Rev.* E **78** (1), 16704.

PRASIANAKIS, N. I., KARLIN, I. V., MANTZARAS, J. & BOULOUCHOS, K. B. 2009 Lattice Boltzmann method with restored Galilean invariance. *Phys. Rev.* E **79** (6), 66702.

RADTKE, G. A. & HADJICONSTANTINOU, N. G. 2009 Variance-reduced particle simulation of the Boltzmann transport equation in the relaxation-time approximation. *Phys. Rev.* E **79** (5), 56711.

RADTKE, G. A., HADJICONSTANTINOU, N. G. & WAGNER, W. 2011 Low-noise Monte Carlo simulation of the variable hard-sphere gas. *Phys. Fluids* **23**, 030606.

SBRAGAGLIA, M., BENZI, R., BIFERALE, L., CHEN, H., SHAN, X. & SUCCI, S. 2009 Lattice Boltzmann method with self-consistent thermo-hydrodynamic equilibria. *J. Fluid Mech.* **628**, 299–309.

SBRAGAGLIA, M. & SUCCI, S. 2005 Analytical calculation of slip flow in lattice Boltzmann models with kinetic boundary conditions. *Phys. Fluids* **17** (9), 93602.

SBRAGAGLIA, M. & SUCCI, S. 2006 A note on the lattice Boltzmann method beyond the Chapman–Enskog limits. *Europhys. Lett.* **73** (3), 370–376.

SCAGLIARINI, A., BIFERALE, L., SBRAGAGLIA, M., SUGIYAMA, K. & TOSCHI, F. 2010 Lattice Boltzmann methods for thermal flows: continuum limit and applications to compressible Rayleigh–Taylor systems. *Phys. Fluids* **22** (5), 55101.

SHAN, X. 1997 Simulation of Rayleigh–Bénard convection using a lattice Boltzmann method. *Phys. Rev.* E **55** (3), 2780–2788.

SHAN, X. 2010 General solution of lattices for Cartesian lattice Bhatanagar–Gross–Krook models. *Phys. Rev.* E **81** (3), 36702.

SHAN, X. & CHEN, H. 2007 A general multiple-relaxation Boltzmann collision model. *Intl J. Mod. Phys.* C **18**, 635–643.

SHAN, X. W. & HE, X. Y. 1998 Discretization of the velocity space in the solution of the Boltzmann equation. *Phys. Rev. Lett.* **80** (1), 65–68.

https://doi.org/10.1017/jfm.2012.616 Published online by Cambridge University Press

SHAN, X. W., YUAN, X. F. & CHEN, H. D. 2006 Kinetic theory representation of hydrodynamics: a way beyond the Navier Stokes equation. *J. Fluid Mech.* **550**, 413–441.

SHIM, J. & GATIGNOL, R. 2011 Thermal lattice Boltzmann method based on a theoretically simple derivation of the Taylor expansion. *Phys. Rev.* E **83** (4), 2–6.

SOFONEA, V. 2009 Implementation of diffuse reflection boundary conditions in a thermal lattice Boltzmann model with flux limiters. *J. Comput. Phys.* **228** (17), 6107–6118.

STRUCHTRUP, H. 2004 Stable transport equations for rarefied gases at high orders in the knudsen number. *Phys. Fluids* **16** (11), 3921–3934.

STRUCHTRUP, H. 2005*a* Derivation of 13 moment equations for rarefied gas flow to second-order accuracy for arbitrary interaction potentials. *Multiscale Model. Simul.* **3** (1), 221–243.

STRUCHTRUP, H. 2005*b* *Macroscopic Transport Equations for Rarefied Gas Flows*. Springer.

STRUCHTRUP, H. & TORRILHON, M. 2003 Regularization of Grad's 13 moment equations: derivation and linear analysis. *Phys. Fluids* **15** (9), 2668–2680.

SUCCI, S. 2002 Mesoscopic modeling of slip motion at fluid-solid interfaces with heterogeneous catalysis. *Phys. Rev. Lett.* **89** (6).

TAHERI, P. & STRUCHTRUP, H. 2010 An extended macroscopic transport model for rarefied gas flows in long capillaries with circular cross section. *Phys. Fluids* **22** (11), 112004.

TAHERI, P., TORRILHON, M. & STRUCHTRUP, H. 2009 Couette and poiseuille microflows: analytical solutions for regularized 13-moment equations. *Phys. Fluids* **21** (1), 017102.

TANG, G. H., GU, X. J., BARBER, R. W., EMERSON, D. R. & ZHANG, Y. H. 2008*a* Lattice Boltzmann model for thermal transpiration. *Phys. Rev.* E **78** (2), 27701.

TANG, G., ZHANG, Y. & EMERSON, D. R. 2008*b* Lattice Boltzmann models for nonequilibrium gas flows. *Phys. Rev.* E **77** (4), 46701.

TIAN, Z.-W., ZOU, C., LIU, H.-J., GUO, Z.-L., LIU, Z.-H. & ZHENG, C.-G. 2007 Lattice Boltzmann scheme for simulating thermal micro-flow. *Physica* A **385** (1), 59–68.

TORRILHON, M. & STRUCHTRUP, H. 2008 Boundary conditions for regularized 13-moment-equations for micro-channel-flows. *J. Comput. Phys.* **227** (3), 1982–2011.

TORO, E. F. 2009 *Riemann Solvers and Numerical Methods for Fluid Dynamics*. Springer.

TOSCHI, F. & SUCCI, S. 2005 Lattice Boltzmann method at finite Knudsen numbers. *Europhys. Lett.* **69** (4), 549–555.

WAGNER, W. 2008 Deviational particle Monte Carlo for the Boltzmann equation. *Monte Carlo Meth. Applic.* **14** (3), 191–268.

WATARI, M. 2009 Velocity slip and temperature jump simulations by the three-dimensional thermal finite-difference lattice Boltzmann method. *Phys. Rev.* E **79** (6), 66706.

WATARI, M. & TSUTAHARA, M. 2003 Two-dimensional thermal model of the finite-difference lattice Boltzmann method with high spatial isotropy. *Phys. Rev.* E **67** (3), 36306.

YUDISTIAWAN, W. P., ANSUMALI, S. & KARLIN, I. V. 2008 Hydrodynamics beyond Navier–Stokes: the slip flow model. *Phys. Rev.* E **78** (1), 16705.

ZHANG, Y., GU, X., BARBER, R. W. & EMERSON, D. R. 2006 Capturing Knudsen layer phenomena using a lattice Boltzmann model. *Phys. Rev.* E **74** (4), 46704.

ZHANG, Y., QIN, R. & EMERSON, D. R. 2005 Lattice Boltzmann simulation of rarefied gas flows in microchannels. *Phys. Rev.* E **71** (4), 47702.

ZHENG, L., GUO, Z., SHI, B. & ZHENG, C. 2010 Kinetic theory based lattice Boltzmann equation with viscous dissipation and pressure work for axisymmetric thermal flows. *J. Comput. Phys.* **229** (16), 5843–5856.

https://doi.org/10.1017/jfm.2012.616 Published online by Cambridge University Press